

Mapping the earthquake-induced landslide hazard around the main oil pipeline network of the Agri Valley (Basilicata, southern Italy) by means of two GIS-based modelling approaches

Flavio Borfecchia¹ · Gerardo De Canio¹ · Luigi De Cecco¹ ·
Alessandro Giocoli¹ · Sergio Grauso¹ · Luigi La Porta¹ ·
Sandro Martini¹ · Maurizio Pollino¹ · Ivan Roselli¹ ·
Alessandro Zini¹

Received: 5 August 2015 / Accepted: 24 November 2015 / Published online: 1 December 2015
© Springer Science+Business Media Dordrecht 2015

Abstract This study presents a first-level spatial assessment of the susceptibility to earthquake-induced landslides in the seismic area of the Agri Valley (Basilicata Region, southern Italy), which hosts the largest onshore oilfield and oil/gas extraction and pre-treatment plant in Europe and is the starting point of the 136-km-long pipeline that transports the plant's products to the refinery located in Taranto, on the Ionian seacoast. Two methodologies derived from the ones proposed by Newmark (Geotechnique 15(2):139–159, 1965) and Rapolla et al. (Eng Geol 114:10–25, 2010, Nat Hazards 61:115–126, 2012. doi:10.1007/s11069-011-9790-z), based on different modelling approaches, were implemented using the available geographic information system tools, which allowed a very effective exploitation of the two models capability for regional zoning of the earthquake-induced landslide hazard. Subsequently, the results obtained from the two models were compared by both visual evaluation of thematic products and statistical correlation analysis of quantitative indices, such as the Safety Index based on the Newmark's approach and the Susceptibility Index from Rapolla's model. The comparison showed a general agreement in highlighting the most critical areas. However, some slight differences between the two models' results were observed, especially where rock materials and steep slopes are prevailing.

Keywords Earthquake-induced landslides · Spatial modelling · Level 1 regional zoning · GIS processing · Lifelines and oil pipelines · Hydrogeological instabilities

✉ Flavio Borfecchia
flavio.borfecchia@enea.it

¹ ENEA, Italian National Agency for New Technologies, Energy and Sustainable Economic Development, Rome, Italy

1 Introduction

Pipelines are main components of the infrastructure that are essential for providing primary social services essential for inhabitants living in urban settlements and for supporting companies and industrial activities. The effect of natural hazards on this type of infrastructures (Hossam and Hossam 2010) is a crucial issue to be considered in order to prevent or mitigate damages to property and people. In the specific case of gas and oil pipelines, the risk arising from the possibility of fire and/or bursts intensifies the potential impact on human casualties, as well as on the loss of infrastructure functionality (Shebeko et al. 2007). Generally, gas/oil pipelines are positioned underground in order to minimize the exposure to weathering and surface accidents. However, relevant ground deformations, such as in earthquake-induced landslides, can affect buried pipelines with potentially dangerous effects.

Important infrastructure for gas/oil extraction and related pipeline networks are located in the valley of the Agri River (Basilicata, southern Italy) and extend to the Taranto oil terminal, in an area characterized by steep slopes in poorly cemented or highly fractured rocks, high slope instability (Vignola et al. 2001) and high seismogenic potential. The combination of all these factors gives rise to a significant earthquake-induced landslide hazard (EILH), a widely used term and concept since a decade (Romeo 2000; Refice and Capolongo 2002; Mahdavifar et al. 2012) at least, which requires spatial assessment and modelling in order to properly address risk facing for mitigation policies and decision-making support in emergency response.

Several methods based on the geographic information system (GIS) spatial modelling approach have been developed for the evaluation of the hazard connected to earthquakes (Borfecchia et al. 2010; Boccardo 2013) and, particularly, to earthquake-triggered landslides (Keefer 1984; Jibson et al. 2000; Rapolla et al. 2010, 2012). Many authors have dealt with post-event inventory assessment and characterization of the earthquake-induced landslides using high-resolution multispectral remotely sensed imagery (Kamp et al. 2010) and in situ georeferenced inspections (Guemache et al. 2010). Some of them have exploited spatial modelling GIS capabilities to assess the seismic landslide hazard by processing topographic and geologic layers within statistical models calibrated by means of an inventory of post-event landslides derived by means of remote sensing in order to obtain semi-quantitative zonation (Kouli et al. 2010; Yang et al. 2014). Fell et al. (2008) suggested three levels of zoning (level 1 regional zoning, scale 1:250,000–1:25,000; level 2 local zoning, scale 1:25,000–1:5,000; and level 3 site-specific zoning, scale > 1:5000) to allow assessment of landslide susceptibility. In this study, the methodologies proposed by Newmark (1965) and Rapolla et al. (2010, 2012) were implemented and GIS tools were used in order to compare their results and to provide a reliable level 1 regional zoning of the susceptibility to earthquake-induced landslides in the area of the gas/oil plant of the Agri Valley.

The selected methods are representative of two different approaches to the estimate of EILH: the first one consists in a permanent-displacement analysis, based on geotechnical-engineering criteria, originally developed to predict the effects of earthquake motion on earth or rock-filled dams and embankments (Newmark 1965); at a later stage, it was adapted and successfully applied to more general problems of slope stability under seismic action (Romeo 2000; Maugeri et al. 2009). Actually, the Newmark's method is halfway between the too simplistic pseudo-static approximation and the overly complex stress–deformation analyses (Jibson 2011). The second method, instead, constitutes a simplified,

typically GIS-based heuristic approach aimed at a quantitative evaluation of the landslide susceptibility in seismic areas. The diverse approaches of these two methods to the EILH evaluation which have been widely applied, mainly singularly, in similar contexts and at various scales, suggested us to test and compare their feasibility and performance in a large-sized seismic area, as that considered here, where, due to the presence of a huge crude oil extraction plant, there is also a stronger commitment at national level.

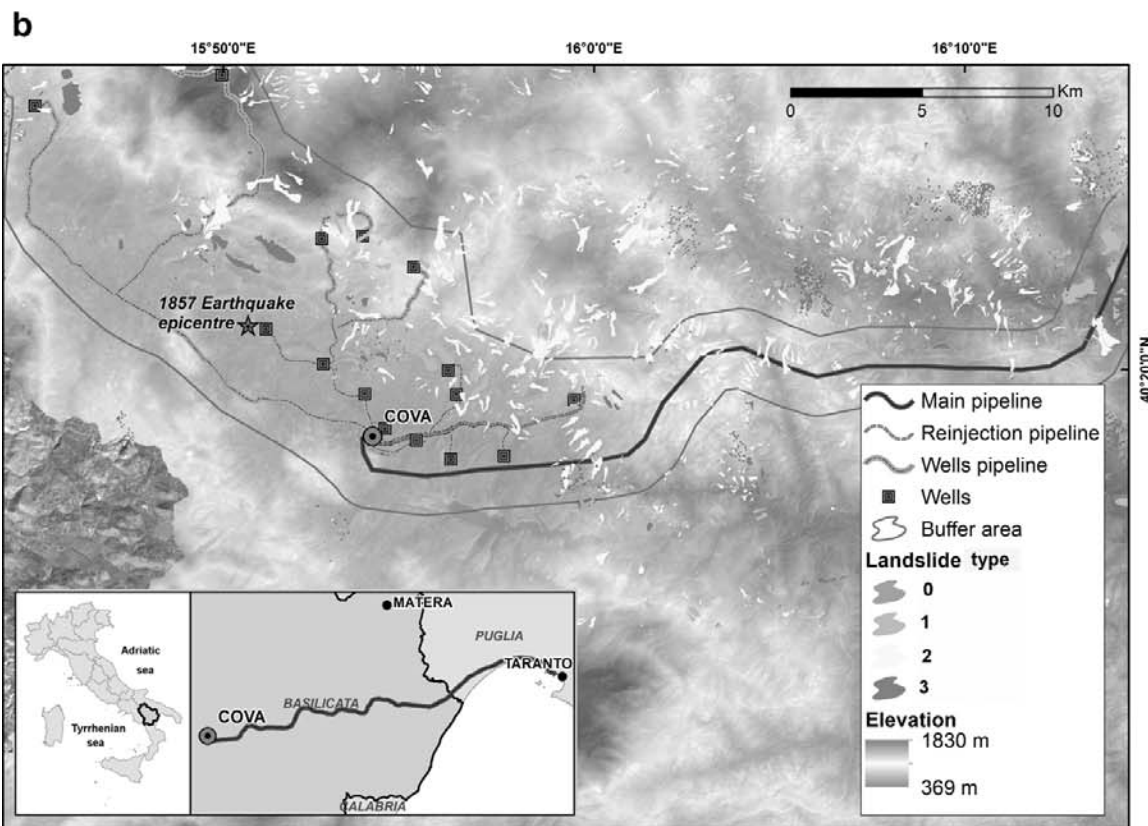
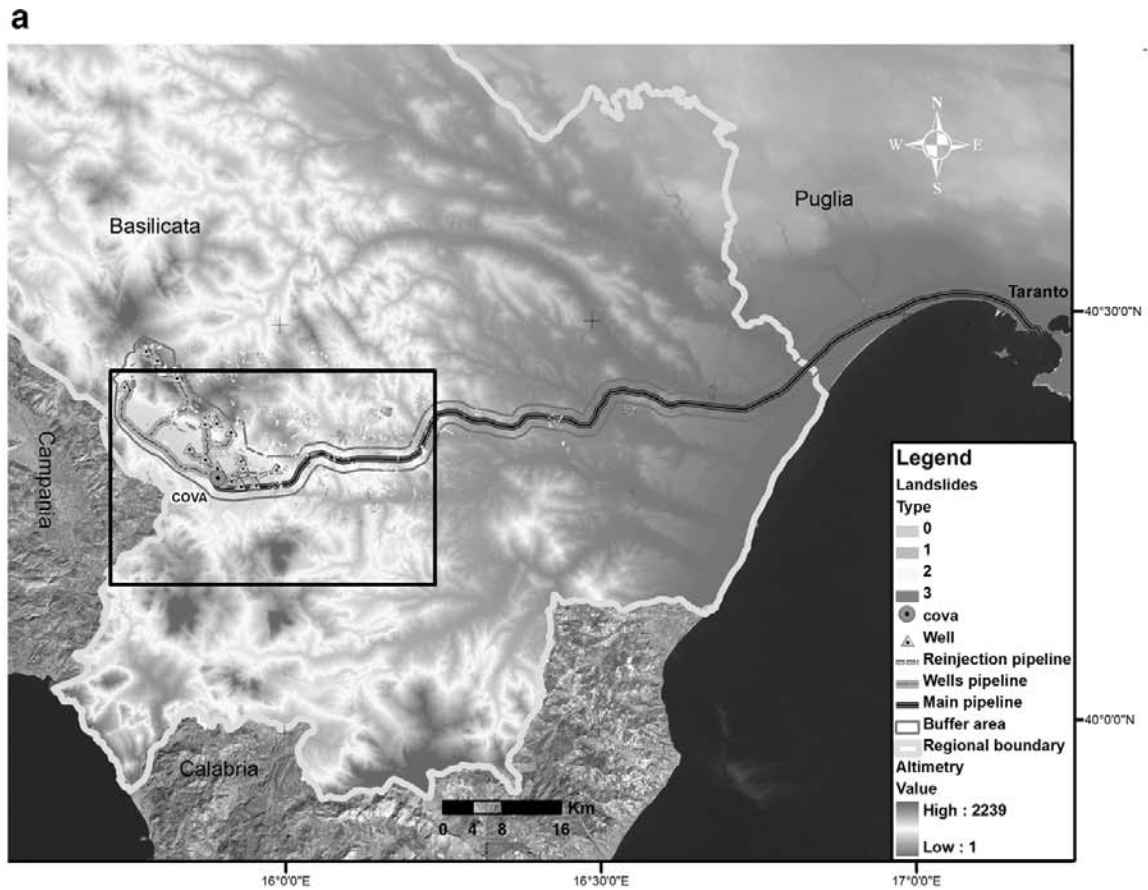
2 Study area

The Upper Agri Valley hosts the largest onshore oilfield and the largest oil/gas pre-treatment plant in Europe, known as Centro Olio Val d'Agri (COVA), managed by ENI Energy Company. At present, there are 25 active productive wells (Ministero dello Sviluppo Economico 2013), which are directly connected to the COVA through a buried pipeline network and reinjection sub-network (Fig. 1). Oil stabilization and gas conditioning are performed at COVA, before piping the oil to the refinery located in Taranto, on the Ionian seacoast, through a 136-km-long, 20-inch-diameter pipeline, referenced as *main pipeline* in Fig. 1. The main pipeline is buried at an average depth of 2 m.

The study area was defined by a 3.0-km-wide buffer area around the above-mentioned gas/oil infrastructures (covering a 61,000 ha area). It crosses the Upper Agri Valley (elevation ranging from about 540 m to about 1835 m above sea level), the valleys of some major Basilicata Rivers (Cavone, Basento and Bradano), and finally reaches the nearly flat landscape of the Ionian seacoast (Fig. 1).

The study area is affected by several natural hazards. From the seismic point of view, the Upper Agri Valley was hit in 1857 by one of the most destructive historical earthquakes in Italy ($M = 7.0$). Conflicting seismogenic models for the Upper Agri Valley are discussed in the recent literature. The seismogenic fault system capable of producing large events is alternatively associated with (1) the Eastern Agri Fault System (EAFS) (Benedetti et al. 1998; Cello et al. 2003; Giano et al. 2000; Giocoli et al. 2015) and (2) the Monti della Maddalena Fault System (MMFS) (Pantosti and Valensise 1990; Maschio et al. 2005; Improta et al. 2010). In addition, Borraccini et al. (2002) supposed that the most probable structure responsible for the development of the active fault system in Agri Valley is a buried fault just below the central part of the valley floor. Many hydrogeological instabilities and landslides have been reported and mapped (e.g. IFFI project—Inventory of Landslide Phenomena in Italy, ISPRA—Servizio Geologico d'Italia 2006) within the area of interest (Fig. 1). The landslides layer reported in Fig. 1 includes the mapped areas in the region of interest affected by these phenomena both with the localization of related triggering points; in addition, the different types of instabilities refer to their level of attention linked to the crossed land cover/use classes derived from CLC2006 (i.e. going respectively from 3 to 0 type number: urban fabric/infrastructures, transportation network, green areas/semi-natural environment, municipality areas without hydrogeological instabilities mapped).

Because of the roughness of relief, the geological features are also quite varied ranging from compact rocks (mainly limestones and sandstones) of Cretaceous–Miocene age in the extraction area, to Plio–Pleistocene poorly cemented sands and clays in the intermediate valleys, to recent alluvial and marine terraced sediments in the final section of the main pipeline. According to the aim of the present study, the spatial analysis was limited to the buffer area potentially involved in earthquake-induced landslide phenomena possibly



◀ **Fig. 1** **a** Map of the infrastructures for gas/oil extraction in the Agri Valley. The map shows the Centro Olio Val d'Agri (COVA), the active productive wells, the main pipeline, the rejection pipeline, the wells pipeline and the buffer area of interest. The map also reports the distribution of landslides (IFFI project—Inventory of Landslide Phenomena in Italy, ISPRA—Servizio Geologico d'Italia 2006); **b** detail of the most critical sector of the study area

affecting the described infrastructure in order to allow the optimization of models implementation and processing time.

3 Data

The available digital terrain model (DTM), geological, geotechnical, seismological and engineering data, mainly under the form of digital maps, were collected from different sources (Table 1) in order to provide the basic input data required by the models. As shown in Fig. 2, the two implemented models share the same databases, consisting in three distinct primary layers: the map of the seismic action, taking into account the site effects (PGA_s); the digital terrain model; and the lithology. The PGA_s (representing the local seismic action) (Fig. 3c) was determined from the PGA (pick ground acceleration, a_g) values of the Italian national scale seismic hazard estimates for the area of interest and in accordance with the latest Italian technical code for construction (NTC 2008) and the Eurocode 8 (2003). The slope steepness map (Fig. 3a) was obtained from a DTM with a 20×20 m mesh. The lithology (Fig. 3b) was derived from the 1:100,000 geological map available at the National Geoportal of the Italian Ministry of the Environment (NG). In particular, the different geological units were assembled in 11 lithological units on the basis of their shear waves velocities (V_s), cohesion (c'), friction angle (ϕ') and unit weight (γ), which were derived from specific literature (e.g. Vignola et al. 2001; Caputo et al. 2004; Maugeri et al. 2005; Caputo et al. 2006; Cherubini et al. 2008; Di Giulio et al. 2008) and in situ investigations, mostly carried out by the administrations of municipalities located in the study area (Table 2). The different parameters of the models were extracted from such three primary layers, as described here forward.

4 Methods

The above-described data were preprocessed and transformed into homogeneous and compatible (in terms of cartographic projection) GIS layers, using specific tools and customized procedures. These layers were combined or merged utilizing specific algorithms to extract or generate the needed information or features mostly in the form of GIS layers (UTM WGS-84 zone 33N cartographic projection). The workflow diagram in Fig. 2 shows the steps followed in generating the EILH maps, while a more detailed schema is reported in appendix (Fig. 7).

According to the NTC (2008), the appropriate levels of protection for the oil pipeline facilities are considered to be achieved by selecting exceedance probabilities (PVR) and return period (RP) as indicated in Table 3 for nominal design life ($V_n \geq 100$ years (large or strategic constructions). For the oil pipeline facilities, a $V_n = 100$ years and a coefficient of use (C_u) equal to 2 were chosen. The probability of exceedance of the seismic action during the $RP = V_n C_u$ varies with the limit state, as shown in Table 3. Therefore,

Table 1 Input layers for GIS modelling

Data layer	Source	Resolution (m)	Scale
Borders Puglia and Basilicata Regions	SINANET		1:10,000
DEM Basilicata	ENEA	20	
DEM Puglia	ENEA	20	
Geologic map Puglia Basilicata	ISPRA		1:100,000
Landslide map Basilicata	ISPRA		1:10,000
Reference PGA on type A ground (a_g)	INGV	<10,000	
COVA map and Viggiano municipal limits	NG		1:10,000
Monte Alpi—Taranto oil pipeline main network	OAVA		1:25,000
Oil pumping stations	OAVA		1:25,000
Wells and reinjection network	OAVA		1:25,000

SINANET is the geographic data repository of the ‘Italian Ministry of the Environment and Protection of Land and Sea’; ENEA is the ‘Italian National Agency for the New Technologies, the Energy and the Sustainable Development’; ISPRA is the ‘Italian Institute for Environmental Protection and Research’; INGV is the ‘Istituto Nazionale di Geofisica e Vulcanologia’; NG is the ‘Italian National Geoportals’; and OAVA is the ‘Osservatorio Ambientale della Val d’Agri’

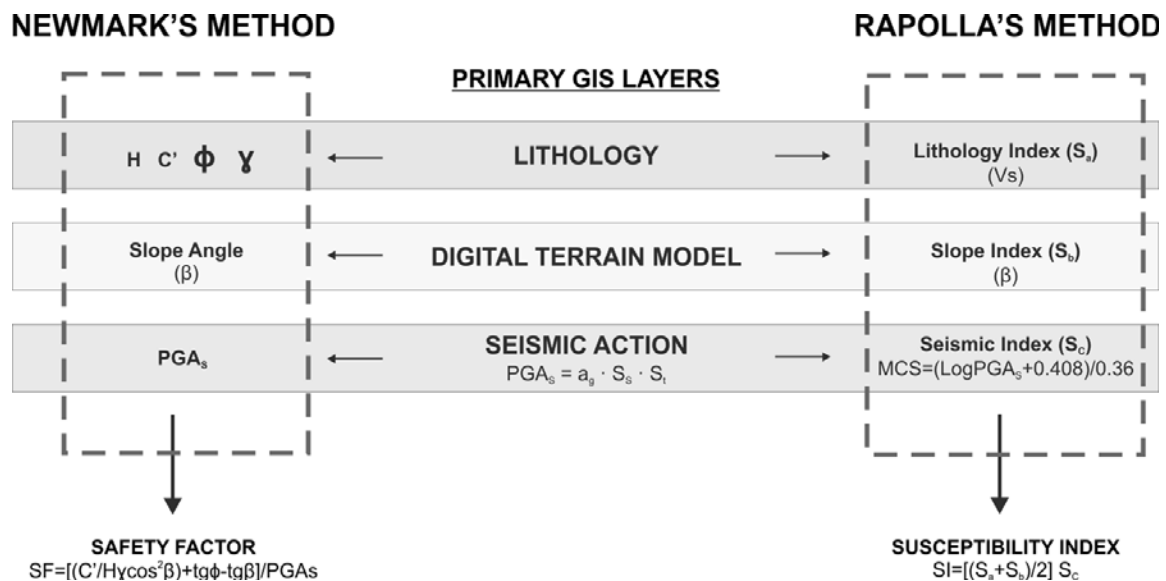


Fig. 2 Synthetic workflow diagram. The *central part* shows the three distinct primary layers common to the two implemented models. On the *left*, the data derived from the primary layers for the Newmark's method. On the *right*, the data derived from the primary layers for the Rapolla's method

for the performance objective SLV (limit state for the safeguard of human life or ultimate state), we produced a seismic hazard map of the area in terms of reference PGA (pick ground acceleration, a_g) on type A ground for RP equal to 1900 years. As the a_g values refer to type A ground (stiff horizontal outcropping bedrock with $V_s > 800 \text{ m s}^{-1}$), the Italian code introduced a stratigraphic factor (S_s) and a topographic factor (S_t) to take account of the site effects. Consequently, the local effective PGA_s to be used as seismic action in our approach is given by the following equation:

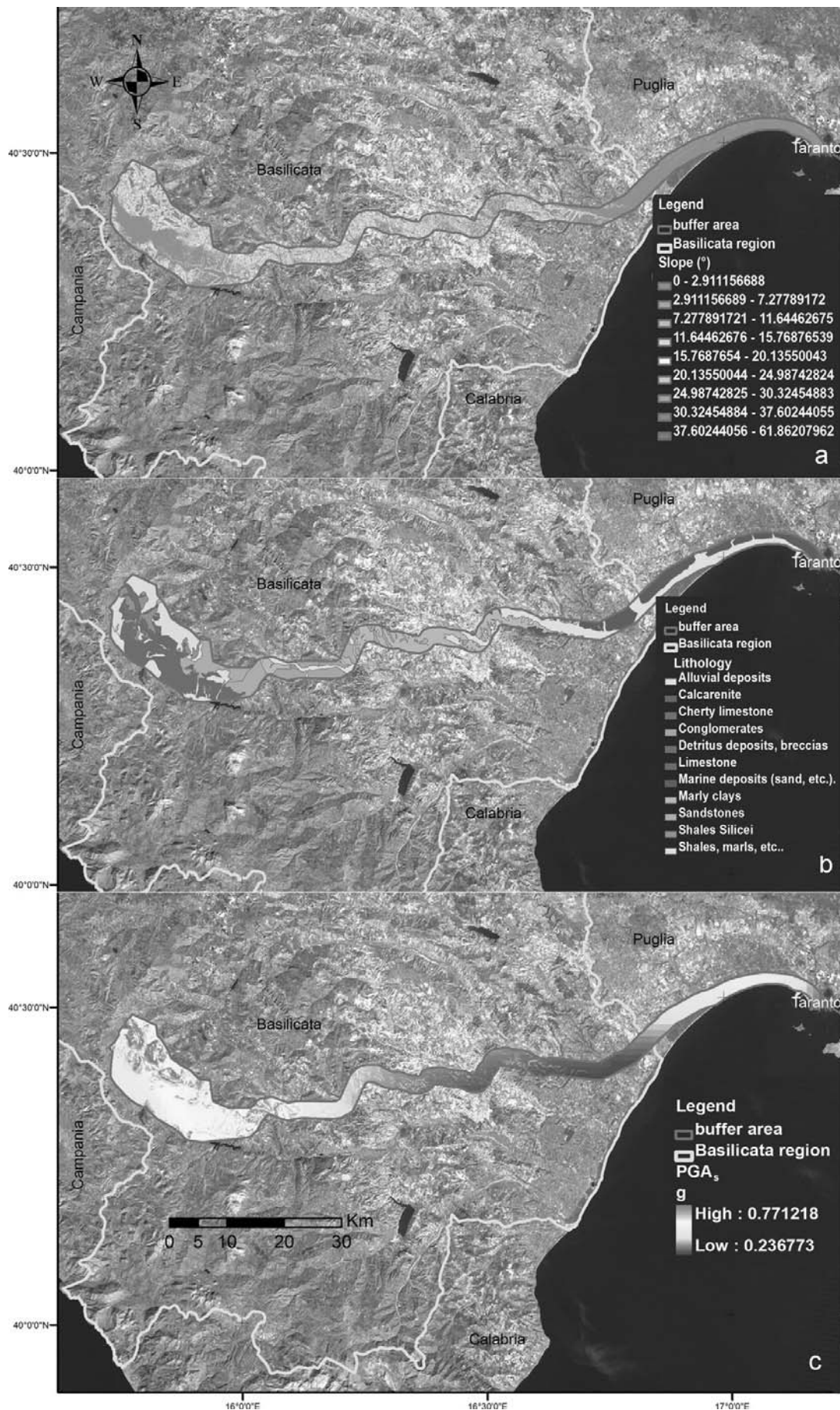


Fig. 3 Intermediate thematic products: **a** slope steepness map; **b** lithological map; and **c** PGAs map

Table 2 Lithologies and related geotechnical parameters

Lithological unit	Rapolla’s method		Newmark’s method	
	V_s (m s ⁻¹)	Cohesion c' (kPa)	Friction angle φ' (°)	Unit weight γ (g cm ⁻³)
Alluvium	250	0	22	1.98
Colluvium and breccia	450	40	25	2.00
Marine deposits	350	0	35	1.84
Conglomerates	550	50	25	1.98
Marly clays	500	45	23	2.05
Sandstones	650	100	28	2.40
Shales, marls, clayey marls and marly limestones	600	150	24	2.00
Siliciferous claystones, marls, marly limestones and fine grained calcarenites	900	260	31	2.60
Calcarenites	800	130	35	2.70
Cherty limestones	1200	315	36	2.55
Platform carbonates	1300	335	38	2.50

Table 3 Seismic action parameters according to the Italian code NTC (2008) (enhanced in light blue are the utilized values)

NTC 2008					
PGA on horizontal seismic bedrock ($V_s > 800$ m/s)	C _u (Coefficient of importance)		2		
	V _n (Nominal design life)		100 yr.		
	V _r (Reference design life) = V _n C _u		200 yr.		
	Performance objective		PVR (exceedance probability)	RP (Return Period)	
	Damage limit states	SLO	81%	RP = 0.6 V _r	120 yr.
		SLD	63%	RP = V _r	200 yr.
Ultimate limit states	SLV	10%	RP = 9.5 V _r	1900 yr.	
	SLC	5%	RP = 19.5 V _r	3900 yr.	
Topographic amplification factor	Features of topography			S _t	
	Plane surface, slope or isolated relief with $\beta \leq 15^\circ$			1.0	
	Slope with $\beta > 15^\circ$			1.2	
	Width of the ridge much lower than width of the toe and $15^\circ \leq \beta \leq 30^\circ$			1.2	
	Width of the ridge much lower than width of the toe and $\beta > 30^\circ$			1.4	
Stratigraphic amplification factor	Ground type			S _s	
	A			1.0	
	B			1.0-1.2	
	C			1.0-1.5	
	D			0.9-1.8	
	E			1.0-1.6	

PGA_s map modulated on the basis of S_t and S_s factors

$$PGA_s = a_g S_s S_t \tag{1}$$

S_s is a function of the ground type, a_g and F₀ (maximum amplification of the horizontal elastic response spectrum). While a_g and F₀ were mapped according to Annex A of NTC (2008) for RP equal to 1900 years, the ground type is supposed to be assigned through seismic microzonation procedure based on V_{s30} measurements. A recent microzonation

project in the region of interest suggested that all landslides areas should be classified as type D ground, since V_{s30} measurements revealed poor indicators on the seismic amplification for this kind of site conditions (Mucciarelli et al. 2006). The above-mentioned project also reported that the presence of zones with many scattered landslides is very common conditions in the study area, as confirmed by the IFFI landslides maps of Basilicata (Fig. 1). Consequently, in the present study S_s was calculated by considering the type D ground (NTC 2008). On the other hand, in the equations provided by the Italian code, taking into account the correlation between F_0 and a_g in the study area (Fig. 4a), S_s decreases with a_g for all ground types so that, in particular, where a_g grows over 0.4 g, S_s values are comprised between 0.9 and 1.1 (Fig. 4b), which means that the soil amplification is weakly dependent on ground types in the most hazardous zones of the study area.

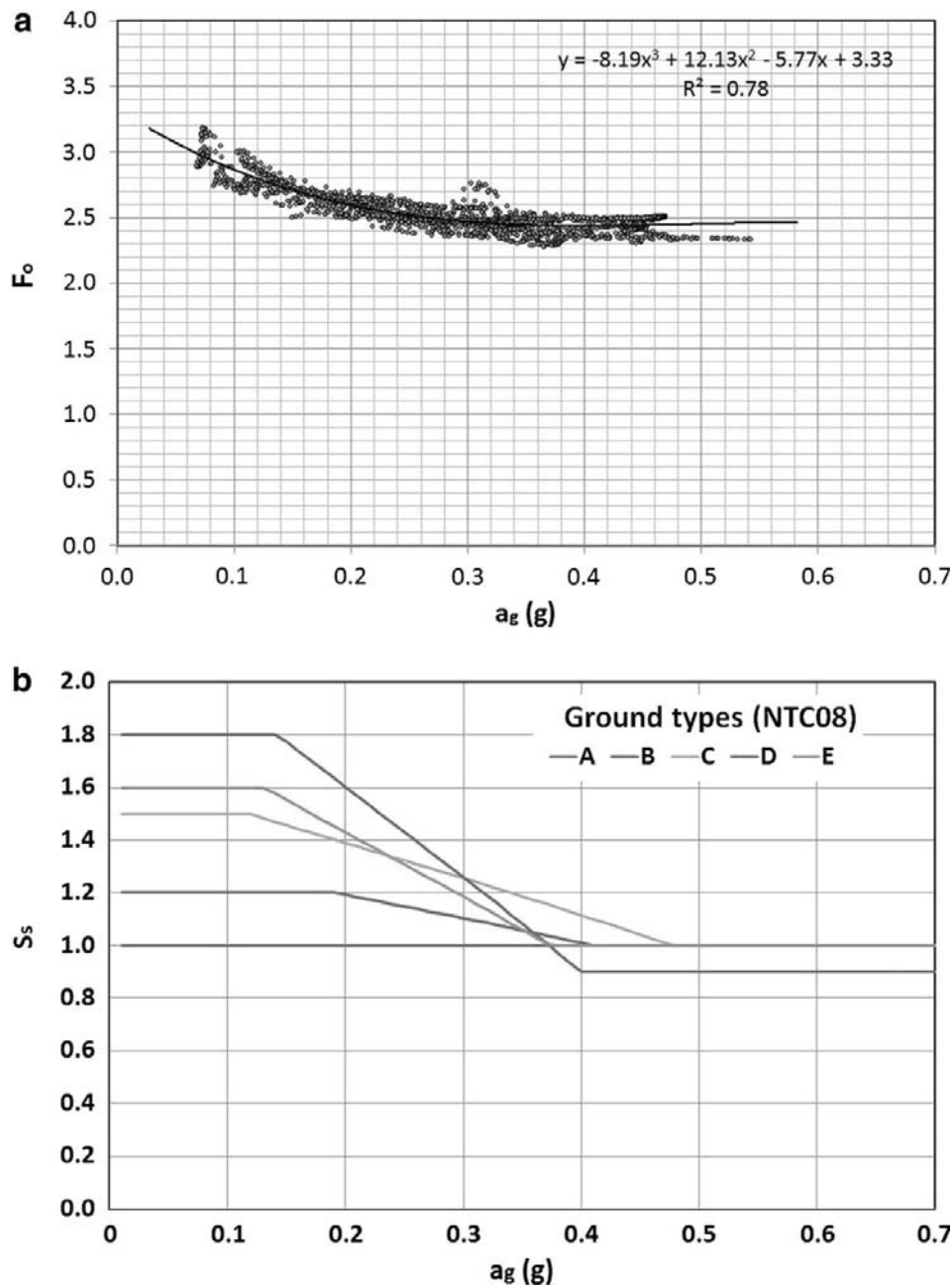


Fig. 4 **a** Correlation between the maximum amplification of the horizontal elastic response spectrum (F_0) and the reference PGA on type A ground (a_g) in the study area. **b** Stratigraphic factor (S_s) versus a_g according to the Italian code NTC (2008)

In addition, the DTM was used to assess the topographic factor S_t by identifying the slope steepness classes and the ridges (Table 3). These latter were obtained by means of the flow direction and basins detection analysis. For each polygonal basin, the minimum and maximum heights (h_{\min} and h_{\max} , respectively) were extracted from the DTM using GIS zonal functions (Fig. 8a in appendix). Then, the following pixel-based interpolation was used:

$$S_t = 1 + b \frac{(h - h_{\min})}{(h_{\max} - h_{\min})} \quad (2)$$

where h is the pixel height and b depends on the slope class (Table 3).

4.1 The Newmark's method

The Newmark's method (Newmark 1965; Maugeri et al. 2009) has undergone several modifications and improvements (Wilson and Keefer 1983) and several relations between seismic ground-motion parameters, and computed landslide displacements have been proposed (Ambraseys and Srbulov 1995; Jibson et al. 2000). In this paper, the simplest model of an infinite slope with a steady sliding surface in dry conditions parallel to the slope was adopted. The critical acceleration coefficient k_y was calculated (Fig. 8b) by the following equation derived from Romeo (2000):

$$k_y = \frac{c'}{H\gamma \cos^2 \beta} + \tan \varphi' - \tan \beta \quad (3)$$

where the critical acceleration ($k_y \times g$) is a function of the geotechnical parameters (c' , φ' and γ), the slope angle β and the depth H of the sliding surface from the ground level. The thickness H of the sliding surface was assumed here equal to 40 m in order to take into account the worst situation from a safety perspective.

Coherently with the Newmark's model, the susceptibility to earthquake-induced landslide was assessed in terms of safety factor SF computed as the ratio of the critical acceleration to the seismic action expressed in terms of PGA_s :

$$SF = \frac{k_y \cdot g}{PGA_s} \quad (4)$$

4.2 The Rapolla's method

Rapolla et al. (2010, 2012) proposed a heuristic approach based on three factors considered significant for predicting the susceptibility to earthquake-induced landslides: the soil/rock geotechnical behaviour (expressed by means of V_s), the slope steepness and the seismic action (PGA_s). The first two factors represent the background predisposing conditions, while the seismic action is the triggering factor for landslide motion.

These factors are synthesized by three indices, respectively: the Lithology Index (S_a); the Slope Index (S_b); and the Seismic Index (S_c). Such indices are comprised between 0 and 1. According to the authors, S_a was computed as a linear function of the inverse of V_s :

$$S_a = \frac{0.2045}{V_s} - 0.1363 \quad (5)$$

S_a is null for $V_s > 1.5 \text{ km s}^{-1}$ (compact, non-fractured rocks) and equal to 1 for $V_s < 0.18 \text{ km s}^{-1}$ (cohesionless or pseudo-coherent clayey materials with high natural

moisture content). The Slope Index, S_b , according to previous studies by Keefer (1984), Mora and Vahrson (1994), Rodriguez et al. (1999) and Wasowski et al. (2002), is modulated on the basis of two distinct proportionality laws valid for soil and rock slopes, respectively:

$$S_b = 0.04 \beta \text{ (soils)} \tag{6}$$

$$S_b = 0.04 \beta - 0.6 \text{ (rocks)} \tag{7}$$

where β = slope (in degrees). On soil slopes, S_b grows linearly from 0 up to the limit value of 25°, over which the value of S_b is kept constant at the maximum value, whereas, on rock slopes, S_b is null for slope angles lower than 15°, and then it grows linearly up to 40° and remains constant at rating 1 for steeper slopes. Finally, the Seismic Index S_c is expressed in terms of the local maximum MCS intensity. Also in this case, a linear relation between S_c and MCS was used. Considering that in the present work the local maximum MCS is equal to XI, the linear equation for the S_c index assumes the following values:

$$S_c = 0.6667(\text{MCS}) - 0.8333 \tag{8}$$

As suggested by the authors, the MCS intensity was derived from the PGA_s (Table 3; Fig. 5b) by means of the formula proposed by Ambraseys (1975):

$$\text{MCS} = \frac{(\log_{10} \text{PGA}_s + 0.408)}{0.36} \tag{9}$$

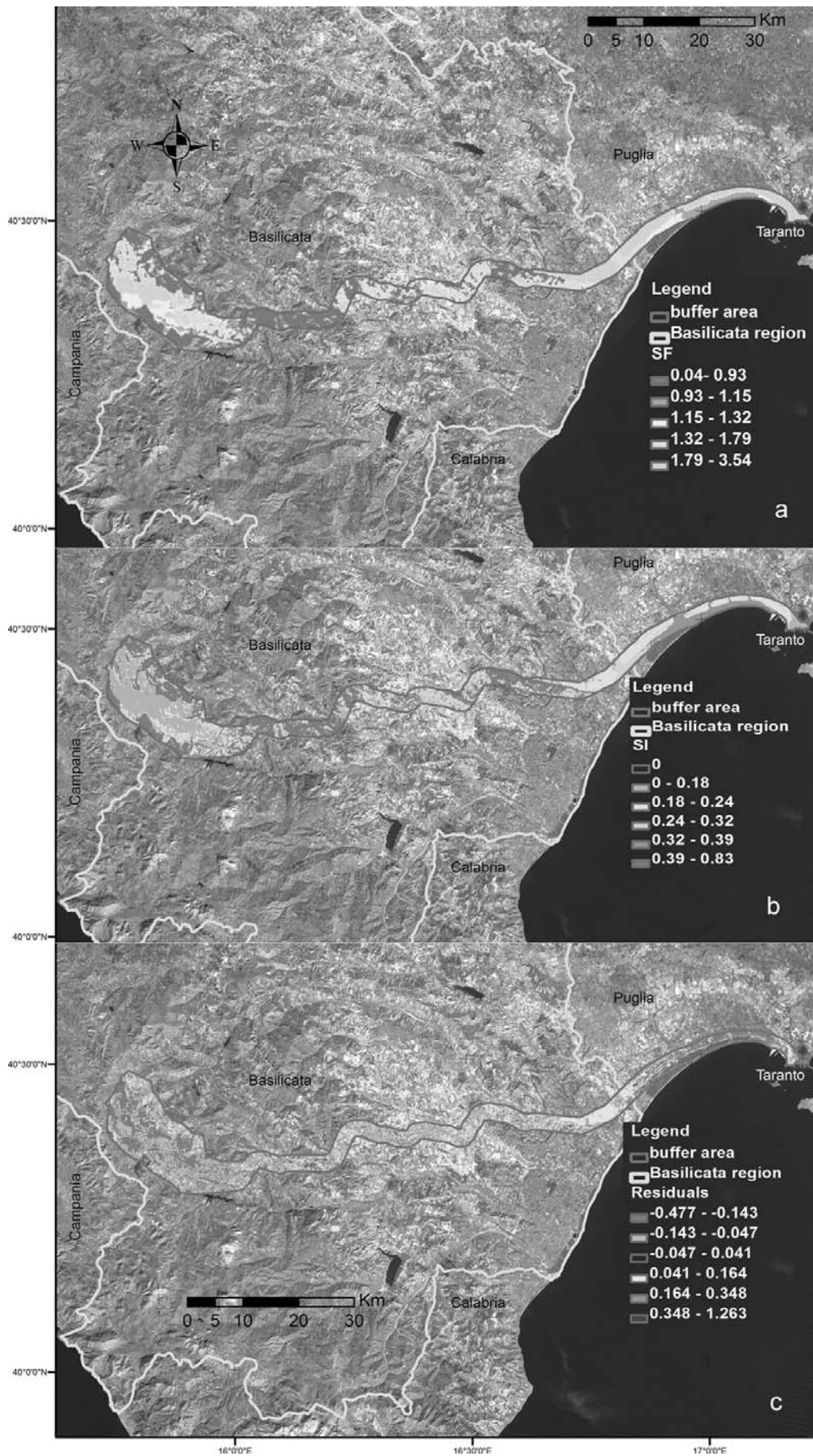
Finally, the seismically induced landslide Susceptibility Index (SI) is obtained by the following equation:

$$\text{SI} = \frac{S_a + S_b}{2} S_c \tag{10}$$

5 Results and discussion

The spatial distributions of SF index and SI in the study area were mapped to emphasize the most critical areas, in terms of EILH, according to the methods of Newmark and Rapolla. In order to obtain an effective zonation, the distributions of SF and SI were represented as five equal-area classes (Table 4), displayed with colour shades from red to green indicating maximum and minimum EILH, respectively (Fig. 5a, b). In this way, SF and SI were classified using the same rules and constraints for the identification of the most critical areas, allowing an inter-comparison, even though the two indices are characterized by different units and mathematical meaning. As shown in Fig. 5, a good global visual agreement between the two zonation maps is evident. In particular, in both maps the most susceptible areas (red zones) are concentrated in the northern and central sectors of the main pipeline and in the oil/gas extraction area (Upper Agri Valley).

In order to have a quantitative comparison, the linear correlation between SF and SI was analysed (Fig. 6). As expected, a significant negative correlation in terms of Pearson’s coefficient was found ($r_{\text{SF,SI}} = -0.654$; $p < 0.001$, i.e. there is a probability that the sample under analysis comes from a population with r value that is due merely to chance). To clarify further, a linear regression model was tested. SF was assumed as dependent variable and SI as explanatory variable. As a whole, the goodness of fit was not very high



◀ **Fig. 5** Final thematic products: **a** safety factor (SF) map; **b** Susceptibility Index (SI) map; and **c** residuals map from linear SF–SI regression model

Table 4 Equal-area zonation limits for SI and SF classifications

Hazard class	SI classification		SF classification	
	Lower limit	Upper limit	Lower limit	Upper limit
Very low	0	0.18	1.79	3.44
Low	0.18	0.24	1.32	1.79
Medium	0.24	0.32	1.15	1.32
High	0.32	0.39	0.93	1.15
Very high	0.39	0.83	0.00	0.93

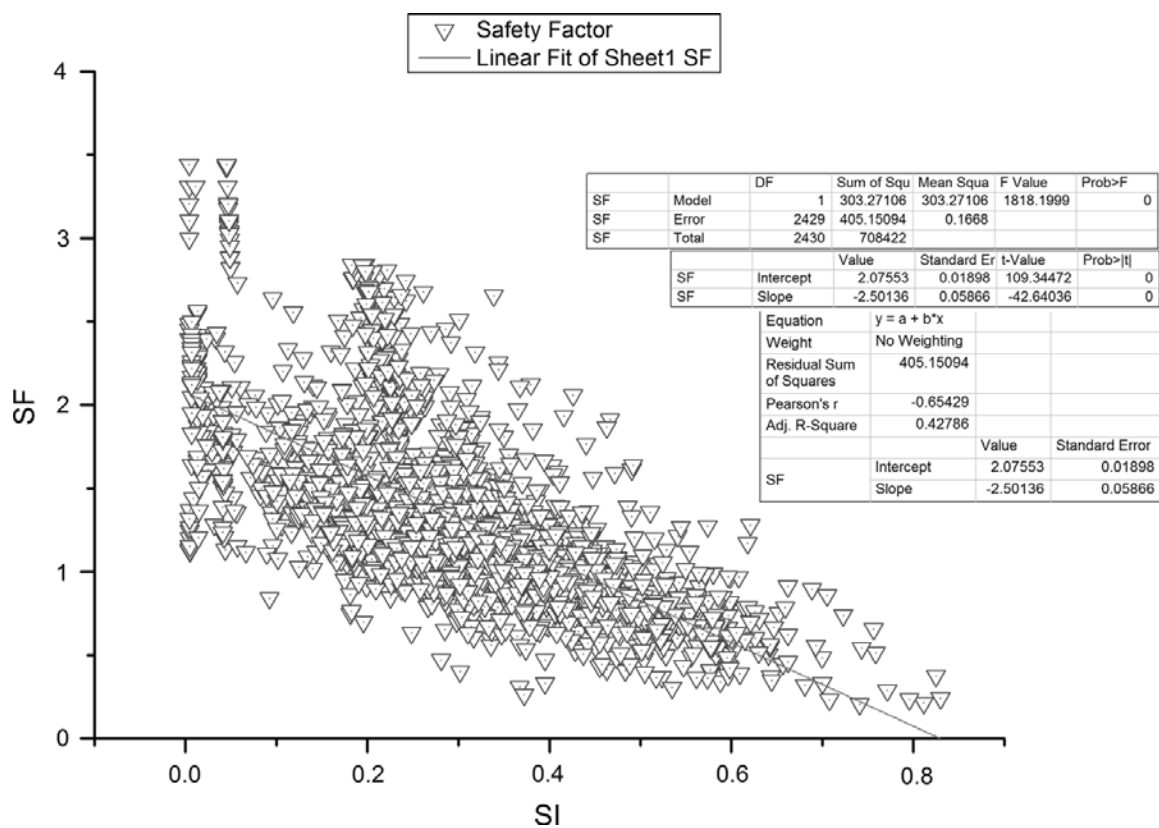


Fig. 6 Linear regression model graph between SF and SI

($R^2 = 0.428$). However, inspecting Fig. 6 it is clear that in correspondence of low SF values in the diagram, the correlation appears weaker and the points look more dispersed. In other words, in spite of a highly significant $r_{SF,SI}$ coefficient, the relation between SF and SI is not linear all over the scatter plot. At the lowest levels of hazard, the range of variation of SF was broader, as evidenced by a ‘flaring’ in the bottom of the graph in Fig. 6. As a consequence, it seemed appropriate to adopt the logarithmic transformation of SF variable. As a matter of fact, a stronger correlation ($r_{SF,SI} = -0.718$; $p < 0.001$) between SI and natural logarithm of SF, along with a lesser dispersion, was obtained. In fact, by reapplying a linear regression model after the aforesaid transformation, the goodness of fit was found better than the previous one ($R^2 = 0.521$). The regression coefficient b_{SI} relative to SI was statistically significant ($b_{SI} = -2.048$; $p < 0.001$,

meaning that the probability that this value is due to chance and is, therefore, equal to zero in the population, is $<1/1000$). It represents the rate of change of SF natural logarithm index as a function of changes in the SI.

Another approach to better understand the degree of agreement between the two indices is the analysis of their five-class distributions. Table 5 shows the contingency matrix based on subdivision into quintiles. The Cohen's kappa coefficient K was estimated on the basis of this matrix (Cohen 1960; Altman 1999). Theoretical K ranges between 0 and 1, with 1 in case of identical classifications, when all the cases are allocated along the diagonal of the contingency table. The estimated global K is rather poor (0.38, see Table 5), but the partial accuracy for the most critical class, marked as *very high* hazard, increases significantly (~ 0.70 , see last row in Table 5, in which a decomposition of global K is showed). The same evidence was achieved by adopting the weighted K indices. The weighting procedure is usually adopted in order to better reflect the ordinal scale measure of the two indices. It minimizes the classification error near the diagonal of the contingency matrix, by attributing higher penalties to misclassifications moving away from the diagonal. In effect, using linear and quadratic weights, the obtained K values were 0.483 and 0.674, respectively, which stand for *moderate* and *good* agreement according to Altman (1999).

Another comparison was carried out by considering the central values of the nominal distributions of the indices (1 and 0.5 for SF and SI, respectively) as a limit between *safe* and *unsafe* zones. The above central values might well represent quite different hazard levels and a better comparison should be based on a deeper knowledge of the indices sensitivity to their input parameters. However, as a first approximation such an assumption can still provide preliminary indications of interest. The related areal extents for both indices were compared. In particular, SI is >0.5 in 8.1 % of the study area, while SF is lower than 1 in 25.9 % of the same area. Therefore, both indices mapped the study area as safe in the great majority of its extent, but Newmark's method seemed to give more conservative results. Possibly, this was due to overly conservative values adopted for particularly uncertain SF input parameters, e.g. the depth H of the sliding surface assumed conservatively equal to 40 m. In any case, the mean values of both indices agreed in indicating an overall safety value (0.241 for SI and 1.347 for SF). A more local evaluation of the results was performed by analysing the distributed residuals arising from the linear regression model (Fig. 5c). The largest disagreements between the SI and SF distributions concentrate mainly in the northern parts of the extraction zone, which are characterized by

Table 5 Contingency matrix for the SI and SF five-class distributions with the estimated Cohen's K coefficients

	SI_Class					Total	K
	Very low	Low	Medium	High	Very high		
SF_Class							
Very low	158	247	49	11	4	469	0.34
Low	178	99	156	64	19	516	0.19
Medium	106	84	143	113	33	479	0.30
High	23	58	116	172	107	476	0.36
Very high	1	9	50	79	352	491	0.72
Total	466	497	514	439	515	2431	
K	0.34	0.20	0.28	0.39	0.68		0.38

very heterogeneous lithology or compact rocks, where Newmark's method, provide extremely conservative outputs due to the previously cited high uncertainty on the input geotechnical parameters values.

6 Conclusions

The GIS spatial modelling approach allowed us to estimate the EILH distribution through SF and SI over the area hosting the most important European onshore gas/oil extraction plant. Two EILH maps of the area of interest were produced on the basis of the models developed by Newmark (1965) and Rapolla et al. (2010, 2012). Although the applied methodologies could not be validated through the comparison of their results with any available in situ data referring to historical earthquake-induced landslides in the study area, both the EILH SF and SI resulting distribution show hazard maxima in correspondence of the areas where landslides are concentrated (e.g. IFFI Project landslide inventory, ISPRA—Servizio Geologico d'Italia 2006) (Fig. 1). The two different approaches were compared for mutual accordancy; in particular, even though the basic models are conceptually different, the results (maps and statistical correlation analysis between SF and SI) showed a substantial agreement in highlighting the most critical areas characterized by high levels of hazard. In addition, the first evaluation of the residual distribution obtained from regression models provided some indications about the input parameters reliability linked to the effective performance of the two exploited modelling methods. The slicing of distributions of both indices into five classes of growing EILH through equal-area zonation produced congruent results, according to Cohen's kappa coefficient K values. These preliminary results demonstrate the capability of both of the utilized GIS-based methods to study the EILH distribution at regional scale (i.e. level 1 zonation).

On the whole, the outcomes from the two implemented models result in satisfying agreement, even if achieved through different conceptual and computational approaches. Only some localized slight disagreements between the two methods were observed, mostly concentrated in the areas characterized by steep rock slopes. Such areas are more difficult to be studied through the Newmark's method, which is indeed particularly appropriate for analysing soil slopes and requires a more accurate geotechnical characterization, more adequate to local and site-specific scale study (level 2 and level 3 of zonation). On the other hand, Rapolla's approach appears easier to apply in providing reliable results at the regional level of our study (level 1 of zonation). As a matter of fact, this method is based on just one geotechnical parameter (V_s) which may be more easily measured by means of in situ surveys or estimated via linked parameters and often is more representative of the overall ground response to seismic shaking at regional scale. The reliability of results coupled with very limited data demand implies a better cost-effective usage of this heuristic method compared with the previous one, based on the displacement analysis, which in any case provided here comparable outcomes.

Considering that the earthquake-induced (or triggered) landslides constitute one of the most dangerous seismic effects, in this earthquake-prone and geologically vulnerable area and generally it is thus of interest to implement an effective modelling approach of the related hazard (EILH) in the prevention and mitigation perspective (i.e. early warning systems). While in general the statistic (multivariate, logistic, etc.) approach has been followed to spatially assess the EILH, here two more physically based models with different capabilities to better account for regional and local responses were implemented and used. While in general these two models have been widely exploited singularly, here they

have been applied both to the same area using the same inputs and this processing schema allowed us to better evaluate their relative intrinsic capabilities and limits by analysing the obtained results. The perspective to include in the present analysis the potential interactions deriving from the impacts of the anthropic extraction activities is one of our future goals.

As a concluding remark, it is worth emphasizing that a first-order assessment of EILH at regional scale can only be a first indicative assessment of the criticalities distribution and that further local investigations should be carried out to provide more representative geological, geomorphological and geotechnical data for proper slope stability modelling and assessment under seismic conditions especially in the field extraction area, more critical also from the geotechnical characterization point of view and seismicity.

Acknowledgments Thanks to Todd Hinkley (Scientist Emeritus—US Geological Survey) for his kind review of the manuscript. Thanks to the anonymous reviewers for their useful suggestions to improve the manuscript. This work was developed in the frame of Project “RoMA” (funded by Italian MIUR SCN_00064 Call “Smart Cities and Communities”) and FP7 Network of Excellence CIPRNet, which is being partly funded by the European Commission under Grant Number FP7-312450-CIPRNet.

Appendix

See Figs. 7 and 8.

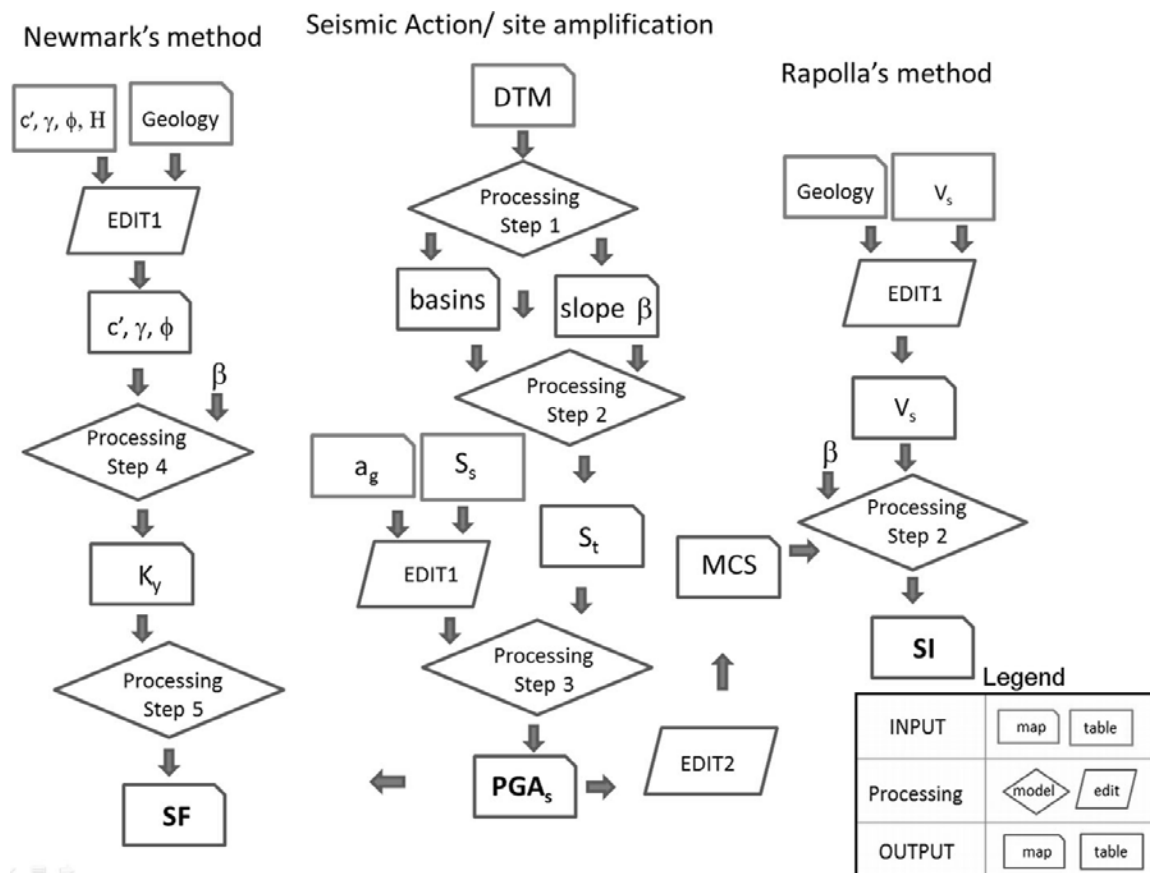


Fig. 7 Detailed workflow schema

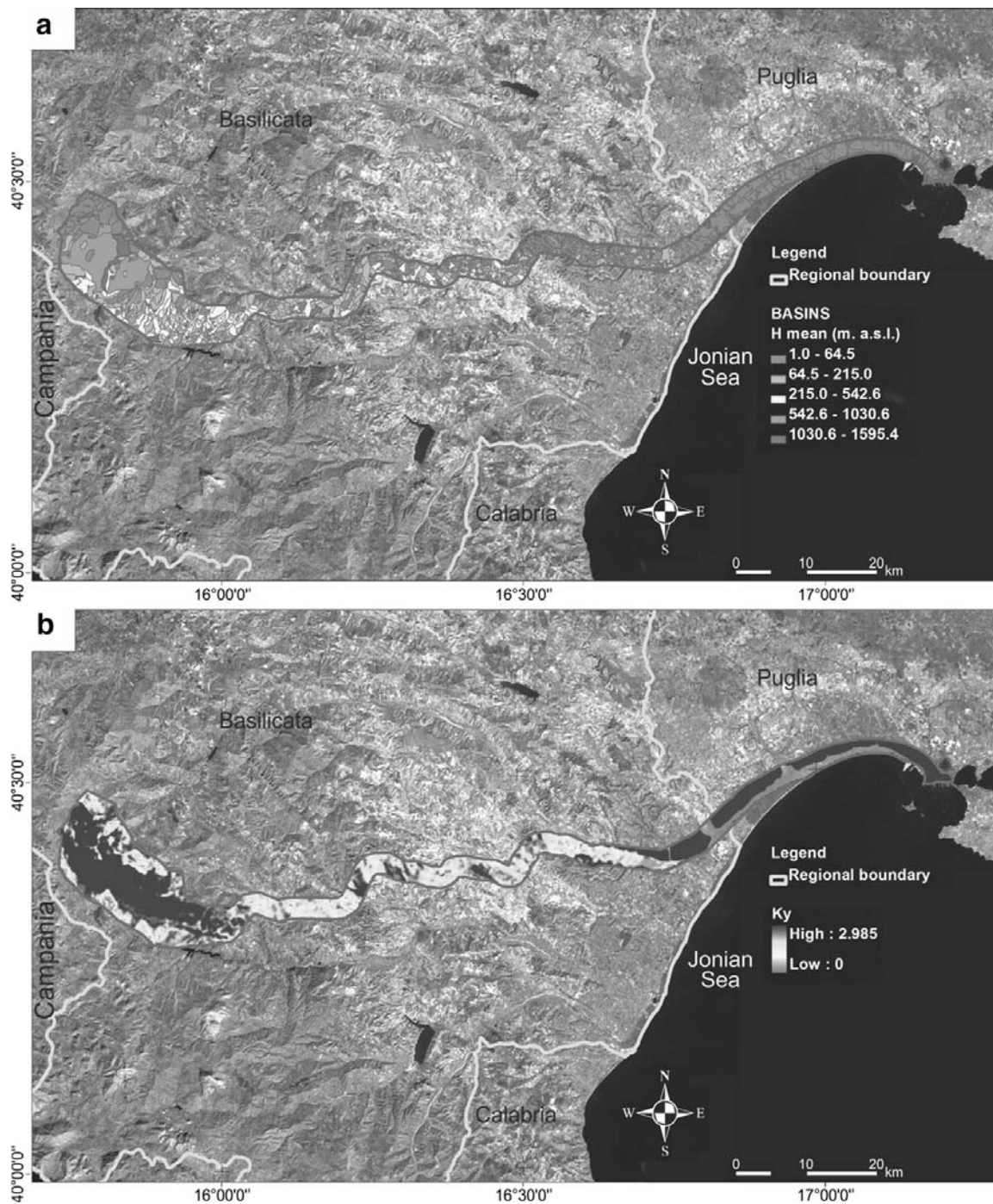


Fig. 8 **a** Sub-basins mean height classes. **b** k_y , critical acceleration coefficient distribution

References

- Altman DG (1999) Practical statistics for medical research. Chapman & Hall/CRC Press, New York
- Ambraseys N (1975) The correlation of intensity with ground motion. In: Proceedings of the XIV General Assembly of the European Seismological Commission, Trieste, 16–22 September 1974, pp 335–341
- Ambraseys N, Srbulov M (1995) Earthquake-induced displacements of slopes. Soil Dyn Earthq Eng 14:59–71. doi:10.1016/0267-7261(94)00020-H
- Benedetti L, Tapponier P, King GCP, Piccardi L (1998) Surface rupture of the 1857 southern Italian earthquake? Terra Nova 10:206–210. doi:10.1046/j.1365-3121.1998.00189.x

- Boccardo P (2013) New perspectives in emergency mapping. *Eur J Remote Sens* 46:571–582. doi:10.5721/EuJRS20134633
- Borfecchia F, De Cecco L, La Porta L, Lugari A, Martini S, Pollino M, Ristoratore E, Pascale C (2010) Active and passive remote sensing for supporting the evaluation of the urban seismic vulnerability. *Ital J Remote Sens* 42:129–141. doi:10.5721/ItJRS201042310
- Borraccini F, De Donatis M, Di Bucci D, Mazzoli S (2002) 3D model of the active extensional fault system of the high Agri River Valley, Southern Apennines, Italy. *J. Virtual Explor.* 6:1–8
- Caputo R, Fiore A, Piedilato S, Sessa R (2004) Analisi dell'amplificazione sismica locale ai fini della pianificazione urbanistica. Caso di studio di Ginestra (PZ) nell'Appennino Meridionale. *Geologia tecnica e ambientale* 1:57–66
- Caputo R, Fiore A, Sessa R (2006) Parametri geologici e territoriali per la pianificazione urbanistica in area sismica. Caso studio di Ripacandida (PZ) nell'Appennino meridionale. *Giornale di Geologia Applicata* 4:189–194. doi:10.1474/GGA.2006-04.0-24.0152
- Cello G, Tondi E, Micarelli L, Mattioni L (2003) Active tectonics and earthquake sources in the epicentral area of the 1857 Basilicata earthquake (Southern Italy). *J Geodyn* 36:37–50. doi:10.1016/S0264-3707(03)00037-1
- Cherubini C, Vessia G, Mannara G, Pingitore D (2008) Valutazione della risposta sismica locale a Sant'Angelo dei Lombardi: il caso dell'ex tribunale. *Giornale di Geologia Applicata* 8(2):177–191. doi:10.1474/GGA.2005-02.0-24.0050
- Cohen J (1960) A coefficient of agreement for nominal scales. *Educ Psychol Meas* 20:37–46. doi:10.1177/001316446002000104
- Di Giulio G, Improta L, Calderoni G, Rovelli A (2008) A study of the seismic response of the city of Benevento (Southern Italy) through a combined analysis of seismological and geological data. *Eng Geol* 97:146–170. doi:10.1016/j.enggeo.2007.12.010
- Eurocode 8 (2003) EN 1998-1, design of structure for earthquake resistance—Part 1: general rules, seismic actions and rules for buildings. CEN European Committee for Standardization, Bruxelles
- Fell R, Corominas J, Bonnard C, Cascini L, Leroi E, Savage WZ (2008) Guidelines for landslide susceptibility, hazard and risk zoning for land use planning. *Eng Geol* 102:85–98
- Giano SI, Maschio L, Alessio M, Ferranti L, Improta L, Schiattarella M (2000) Radiocarbon dating of active faulting in the Agri high valley, Southern Italy. *J Geodyn* 29:371–386
- Giocoli A, Stabile TA, Adurno I, Perrone A, Gallipoli MR, Gueguen E, Norelli E, Piscitelli S (2015) Geological and geophysical characterization of the southeastern side of the High Agri Valley (southern Apennines, Italy). *Nat Hazards Earth Syst* 15:315–323. doi:10.5194/nhess-15-315-2015
- Guemache MA, Machane D, Beldjoudi H, Gharbi S, Djadia L, Benahmed S, Ymmel H (2010) On a damaging earthquake-induced landslide in the Algerian Alps: the March 20, 2006 Laâlam landslide (Babors chain, northeast Algeria), triggered by the Kherrata earthquake (Mw 5.3). *Nat Hazards* 54:273–288. doi:10.1007/s11069-009-9467-z
- Hossam AK, Hossam AG (2010) Review of pipeline integrity management practices. *Int J Press Vessels Pip* 87:373–380. doi:10.1016/j.ijpvp.2010.04.003
- Improta L, Ferranti L, de Martini PM, Piscitelli S, Bruno PP, Burrato P, Civico R, Giocoli A, Iorio M, D'addezio G, Maschio L (2010) Detecting young, slow-slipping active faults by geologic and multi-disciplinary high-resolution geophysical investigations: a case study from the Apennine seismic belt, Italy. *J Geophys Res* 115:B11307. doi:10.1029/2010JB000871
- ISPRA—Servizio Geologico d'Italia (2006) Progetto IFFI (Inventario dei Fenomeni Franosi in Italia). Landslide Inventory Map of Italy at 1:25,000 scale. ISPRA—Dipartimento Difesa del Suolo-Servizio Geologico d'Italia—Regione Campania (www.sinanet.apat.it/progettoiffi)
- Jibson RW (2011) Methods for assessing the stability of slopes during earthquakes—a retrospective. *Eng Geol* 122:43–50
- Jibson RW, Harp EL, Michael JA (2000) A method for producing digital probabilistic seismic landslide hazard maps. *Eng Geol* 58:271–289. doi:10.1016/S0013-7952(00)00039-9
- Kamp U, Owen LA, Growley BJ, Khattak AG (2010) Back analysis of landslide susceptibility zonation mapping for the 2005 Kashmir earthquake: an assessment of the reliability of susceptibility zoning maps. *Nat Hazards* 54:1–25. doi:10.1007/s11069-009-9451-7
- Keefer DK (1984) Landslides caused by earthquakes. *Geol Soc Am Bull* 95:406–421. doi:10.1130/0016-7606(1984)95<406:LCBE>2.0.CO;2
- Kouli M, Loupasakis C, Soupios P, Vallianatos F (2010) Landslide hazard zonation in high risk areas of Rethymno Prefecture, Crete Island, Greece. *Nat Hazards* 52:599–621. doi:10.1007/s11069-009-9403-2
- Mahdaviifar M, Memarian P, Manjil R (2012) Assessment of earthquake-induced landslides triggered by earthquake in Rostamabad(Iran) quadrangle using knowledge-based hazard analysis approach. In:

- Keizo U, Hiroshi Y, Akihiko W (eds) Proceedings of the International Symposium on Earthquake-Induced Landslides, Kiryu, Japan, pp 769–780. ISBN 978-3-642-32238-9
- Maschio L, Ferranti L, Burrato P (2005) Active extension in Val d’Agri area, Southern Apennines, Italy: implications for the geometry of the seismogenic belt. *Geophys J Int* 162:591–609. doi:10.1111/j.1365-246X.2005.02597.x
- Maugeri M, Mussumeci G, Biondi G, Condorelli A (2005) Strumenti di analisi e metodologie di rappresentazione in un SIT “specializzato” sul rischio sismico di frana. *Boll SIFET* 1(2005):53–70 (in Italian)
- Maugeri M, Motta E, Mussumeci G, Raciti E (2009) Lifeline seismic hazards: a GIS application. *WIT Trans Built Environ* 104:381–392. doi:10.2495/ERES090351
- Ministero dello Sviluppo Economico (2013) Executive summary of DGRME annual report 2013—year 2012. <http://unmig.sviluppoeconomico.gov.it/unmig/stat/ra2013eng.pdf>
- Mora S, Vahrson W (1994) Macrozonation methodology for landslide hazard determination. *Bull Int As Eng Geol* 31(1):49–58
- Mucciarelli M, Caputo V, Sdao F, Gallipoli M.R, Giano S.I, Bianca M, Bulfaro M, Camassi R, Lopiano M, Lizza C, Bruno G (2006) Convenzione tra Regione Basilicata e Di.S.G.G.-Università della Basilicata per la realizzazione del progetto di monitoraggio geofisico e di amplificazione sismica di sito di aree vulnerabili del territorio regionale. Relazione Finale Preliminare 08/10/02-31/07/05. http://www.crisbasilicata.it/microzonazione/documenti/Rapporto_finale_Microzonazione_rev2.pdf (in Italian)
- Newmark NM (1965) Effects of earthquakes on dams and embankments. *Geotechnique* 15(2):139–159
- N.T.C (2008) Approvazione delle nuove norme tecniche per le costruzioni (Italian Building Code). *Gazzetta Ufficiale della Repubblica Italiana*, n. 29 del 4 febbraio 2008—Suppl. Ordinario n. 30, 2008 (in Italian)
- Pantosti D, Valensise G (1990) Faulting mechanism and complexity of the November 23, 1980, Campania-Lucania earthquake, inferred from surface observation. *J Geophys Res* 95:15319–15341
- Rapolla A, Paoletti V, Secomandi M (2010) Seismically-induced landslide susceptibility evaluation: application of a new procedure to the island of Ischia, Campania Region, Southern Italy. *Eng Geol* 114:10–25. doi:10.1016/j.enggeo.2010.03.006
- Rapolla A, Di Nocera S, Matano F, Paoletti V, Tarallo D (2012) Susceptibility regional zonation on earthquake-induced landslide in Campania, Southern Italy. *Nat Hazards* 61:115–126. doi:10.1007/s11069-011-9790-z
- Refice A, Capolongo D (2002) Probabilistic modeling of uncertainties in earthquake-induced landslide hazard assessment. *Comput Geosci* 28(6):735–749
- Rodriguez CE, Bommer JJ, Chandler RJ (1999) Earthquake-induced landslides: 1980–1997. *Soil Dyn Earthq Eng* 18:325–346. doi:10.1016/S0267-7261(99)00012-3
- Romeo R (2000) Seismically induced landslide displacements: a predictive model. *Eng Geol* 58:337–351. doi:10.1016/S0013-7952(00)00042-9
- Shebeko YN, Bolodian IA, Molchanov VP, Deshevih YI, Gordienko DM, Smolin IM, Kirillov DS (2007) Fire and explosion risk assessment for large-scale oil export terminal. *J Loss Prev Process* 20:651–658. doi:10.1016/j.jlp.2007.04.008
- Vignola N, Tramutoli M, Melfi D (2001) Analisi del dissesto da frana in Basilicata. Progetto IFFI, Conv. Reg. Basilicata n. DSTN/27 7885. <http://www.isprambiente.gov.it/files/pubblicazioni/rapporti/rapporto-frane/capitolo-22-basilicata.pdf> (in Italian)
- Wasowski J, del Gaudio V, Pierri P, Capolongo D (2002) Factors controlling seismic susceptibility of the Sele Valley slopes: the case of the 1980 Irpinia earthquake re-examined. *Surv Geophys* 23:563–593. doi:10.1023/A:1021230928587
- Wilson RC, Keefer DK (1983) Dynamic analysis of a slope failure from the 6 August 1979 Coyote Lake, California, earthquake. *Bull Seismol Soc Am* 73:863–887
- Yang Z, Lan H, Gao X, Li L, Meng Y, Wu Y (2014) Urgent landslide susceptibility assessment in the 2013 Lushan earthquake-impacted area, Sichuan Province, China. *Nat Hazards*. doi:10.1007/s11069-014-1441-8